Materials Science and Engineering A 527 (2010) 7832–7840

Contents lists available at ScienceDirect

Materials Science and Engineering A

journal homepage: www.elsevier.com/locate/msea

Effect of grain refinement to 1 μm on strength and toughness of dual-phase steels

Marion Calcagnotto*, Dirk Ponge, Dierk Raabe

Max-Planck-Institut für Eisenforschung GmbH, Max-Planck-Straße 1, 40237 Düsseldorf, Germany

ARTICLE INFO

Article history:
Received 16 June 2010
Received in revised form 19 August 2010
Accepted 24 August 2010

Keywords:
Grain refinement
Dual-phase steel
Ultrafine grains
Toughness
Warm deformation

ABSTRACT

Large strain warm deformation at different temperatures and subsequent intercritical annealing has been applied to obtain fine grained (2.4 μm) and ultrafine grained (1.2 μm) ferrite/martensite dual-phase (DP) steels. Their mechanical properties were tested under tensile and impact conditions and compared to a hot deformed coarse grained (12.4 μm) reference material. Both yield strength and tensile strength follow a Hall–Petch type linear relationship, whereas uniform elongation and total elongation are hardly affected by grain refinement. The initial strain hardening rate as well as the post-uniform elongation increase with decreasing grain size. Ductile fracture mechanisms are considerably promoted due to grain refinement. Grain refinement further lowers the ductile-to-brittle transition temperature and leads to higher absorbed impact energies. Besides the common correlations with the ferrite grain size, these phenomena are explained in terms of the martensite particle size, shape and distribution and the more homogeneous dislocation distribution in ultrafine ferrite grains.

1. Introduction

Dual-phase (DP) steels consisting of a soft ferrite matrix and typically 5–30 vol.% of hard martensite particles combine high strength with good formability and weldability. Therefore, they are widely used for automotive applications. Since their development four decades ago, the microstructure–property relationships have been extensively studied [1–13]. In view of the increasing demands for occupant safety and fuel efficiency, further strengthening of DP steels without a loss in ductility is required. Grain refinement is a promising tool to achieve this aim [14–19]. In the early studies on the grain size effect in DP steels [14,15], the minimum ferrite grain size was around 5 μm due to limitations of the conventional thermomechanical processing routes. In recent years, a variety of new processing routes has been developed to produce ultrafine grained (UFG) low carbon steels with a ferrite grain size of 1 μm and below [20].

UFG DP steels with a ferrite grain size around 1 μm have been produced by applying a two-step processing route consisting of (1) a deformation treatment to produce UFG ferrite and finely dispersed cementite or pearlite and (2) a short intercritical annealing in the ferrite/austenite two-phase field followed by quenching to transform all austenite to martensite. Grain refinement in step (1) was achieved by equal channel angular pressing (ECAP) [16], cold rolling [17] and cold swaging [18]. A single-pass processing route based on deformation induced ferrite transformation (DIFT) was proposed by Mukherjee et al. [21]. It was consistently found that yield strength and tensile strength are increased due to grain refinement, whereas uniform and total elongation are less affected. The strain hardening rate was found to increase with decreasing grain size [16] which is in contrast to the observation of the very restricted strain hardening rate in UFG low carbon ferrite/cementite steels [22,23]. As the number of investigations on this topic is very limited, a better understanding of the mechanical response of DP steels to ferrite grain sizes close to or below 1 μm is required.

In contrast to other methods to increase the strength of steels, grain refinement simultaneously improves the toughness of the material, i.e. its capability to absorb energy under impact conditions. Several studies on UFG ferrite/cementite steels revealed that the ductile-to-brittle transition temperature (DBTT) is significantly reduced due to grain refinement, e.g. [24–26]. However, the grain size dependence of the impact properties of UFG DP steels has not been addressed up to now.

The most distinct mechanical properties of DP steels are the low elastic limit, the high initial strain hardening and the overall continuous yielding in the quenched state. These features have been attributed to residual stresses and dislocation heterogeneities present in the ferrite as a result of the austenite-to-martensite transformation [27–30]. This transformation involves a volume expansion of 2–4%, depending on chemical composition [31], causing an elastically and plastically deformed zone in the ferrite adjacent to martensite [7,32,33]. The elastic stresses facilitate plastic flow during the early stages of yielding. Dislocation–dislocation interaction, dislocation pile-ups at ferrite/martensite interfaces and

* Corresponding author. Tel.: +49 211 6792 416; fax: +49 211 6792 333.
E-mail addresses: m.calcagnotto@mpie.de (M. Calcagnotto), d.ponge@mpie.de (D. Ponge), d.raabe@mpie.de (D. Raabe).

0921-5093/$ – see front matter © 2010 Elsevier B.V. All rights reserved.
doi:10.1016/j.msea.2010.08.062

the corresponding long-range elastic back stresses contribute to rapid strain hardening [4,28]. However, it is not clear to which extent this theory applies to UFG ferrite. Clearly, the dislocation distribution is different in UFG ferrite and consequently, the deformation mechanisms might change.

This study aims at a detailed description of the tensile and impact properties of three DP steels having the same chemical composition but different grain sizes. Unlike in previous studies, the materials presented in this study have roughly the same martensite volume fraction and the same martensite carbon content, so that the individual effect of grain refinement on the overall mechanical properties can be studied more consistently, without the simultaneous change of other microstructure features.

2. Experimental procedures

The chemical composition of the steel used was (in wt.%) 0.17 C, 1.49 Mn, 0.22 Si, 0.033 Al, 0.0033 N, 0.0017 P and 0.0031 S. A lean composition was chosen in order to show that a stable ferrite grain size of around 1 μm can be achieved via thermomechanical processing without the addition of expensive grain growth inhibitors like vanadium or niobium. Previously, it was shown that a certain manganese content is highly beneficial for the grain refining process [34] and essential to achieve sufficient hardenability [35]. The steel was produced by vacuum induction melting. Samples (50 mm × 40 mm × 60 mm) were machined directly from the cast ingot. The thermomechanical processing was realized by use of a large scale 2.5 MN hot deformation simulator located at the Max-Planck-Institut für Eisenforschung [36–38]. This computer controlled servohydraulic press allows to simulate industrial hot rolling processing routes by performing multi-step flat compression tests. The processing schedules to obtain different grain sizes are outlined in Fig. 1. Austenitization at 912 °C for 3 min and subsequent deformation at 860 °C (with a logarithmic strain of $\varepsilon = 0.3$ at a strain rate of $10\,s^{-1}$) produces fully recrystallized austenite which transforms into relatively coarse grained (CG) ferrite and pearlite upon slow cooling, Fig. 1a. Grain refinement is achieved by subsequent warm deformation exerting a four-step flat compression series with a strain of 0.4 per step, an interpass time of 0.5 s and a strain rate of $10\,s^{-1}$. The deformation temperature controls the degree of grain refinement. At 700 °C (Fig. 1b), a fine grained (FG) polygonal ferrite matrix is obtained with small islands of pearlite and globular cementite (FG-route). At 550 °C (Fig. 1c), the ferrite is refined to around 1 μm (which is referred to as UFG ferrite) due to grain subdivision and pronounced recovery [39,38]. The cementite lamellae of the pearlite colonies undergo continuous fragmentation and spheroidization. After a total strain of 1.6, pearlite is completely replaced by spheroidized sub-μm sized cementite which is distributed homogeneously along the ferrite grain boundaries (UFG-route). After warm deformation, specimens were annealed for 2 h at the respective deformation temperature to simulate elevated coiling temperatures. Details about the microstructure evolution during warm deformation and annealing at 550 °C are given in Ref. [38]. To obtain the final ferrite/martensite dual-phase microstructure the specimens were subjected to intercritical annealing in a salt bath furnace. The temperature was controlled electronically and held constant at 730 °C. The samples were annealed for 3 min (including reheating time) in the salt bath, before they were quenched in water to obtain a ferrite/martensite DP structure. These parameters were established by performing dilatometer tests [35].

Cylindrical tensile test specimens with a diameter of 4 mm and a gage length of 20 mm were machined according to the German Industry Norm DIN 50125-B. Tensile tests were conducted at room temperature with a constant cross-head speed of 0.5 mm/min and an initial strain rate of $0.5 \times 10^{-3}\,s^{-1}$. Due to the continuous yielding behavior, the yield strength is given as the 0.2% offset yield strength. The uniform elongation was determined as the strain at which the true strain equals the strain hardening rate (Considère criterion). The strain hardening exponent, n, was determined as an approximation to the Hollomon equation ($\sigma_t = k\varepsilon_t^n$, where σ_t is the true stress, ε_t is the true strain and k is an empirical constant) between 2% and uniform elongation. The reduction in area was determined by measuring the area of the fracture surface related to the initial surface.

V-notched specimens test were cut along the rolling direction with a cross section of 3 mm × 4 mm according to the German Industry Norm DIN 50115. The notch was placed 10 mm from the center of the sample where the local strain equals the nominal strain [40]. Impact tests were carried out in a temperature range of −40 to 200 °C. The temperature was controlled by a thermocouple welded on the specimen surface. The ductile-to-brittle transition temperature (DBTT) was determined using two different approaches. First, it was measured as the temperature corresponding to the half value of the upper shelf energy (USE), determined from the Charpy impact curve. Second, it was defined as the temperature at which 50% of fracture is of brittle type, observed by electron microscopy. The latter is the fracture appearance transition temperature (50%-FATT). The USE and the DBTT obtained using subsize specimen are smaller than the values obtained using fullsize specimen because of the reduced specimen cross section and the different stress state. Kaspar and Faul [41] conducted a comparative study on normalized ferrite/pearlite steels with several chemical compositions and found linear relations of the USE and the DBTT to hold between subsize and fullsize specimen. Although the steel investigated in the present study is different, their correlations are used here as a first approximation to convert the USE and the DBTT to the respective values of conventional Charpy V-notch specimens.

Samples for scanning electron microscopy (SEM) were prepared by standard mechanical grinding and polishing procedures, finishing with 3 min colloidal silica polishing. To reveal the microstructure, the samples were additionally etched in 1% Nital for 3 s.

The martensite volume fraction and the ferrite grain size were determined on the basis of three SEM micrographs taken at a magnification of 3000× for the UFG and FG steel and of 500× for the CG steel. The point counting method was used to determine the second-phase fraction. As it is not possible to differentiate between martensite and austenite on etched specimens in the SEM, the second-phase fraction was determined as the fraction of martensite plus retained austenite. The retained austenite volume fraction was determined to range between 1 and 3 vol.% based on electron backscatter diffraction (EBSD) measurements. The ferrite mean linear intercept (MLI) length was determined both in the compression direction and in the rolling direction. The average value determines the ferrite grain size.

3. Results

3.1. Microstructures

The microstructure obtained after hot deformation and air cooling followed by intercritical annealing (CG-route) consists of a ferrite matrix with a grain size of 12.4 μm and 31.3% martensite, Table 1, the latter occurring partly as isolated islands, partly as aligned bands. By applying multi-pass warm deformation at 700 °C (FG-route) and 550 °C (UFG-route) between hot deformation and intercritical annealing, the ferrite grain size is reduced to 2.4 and 1.2 μm, respectively. The martensite fraction is 30.1 vol.% in the FG steel and 29.8 vol.% in the UFG steel. The martensite islands are

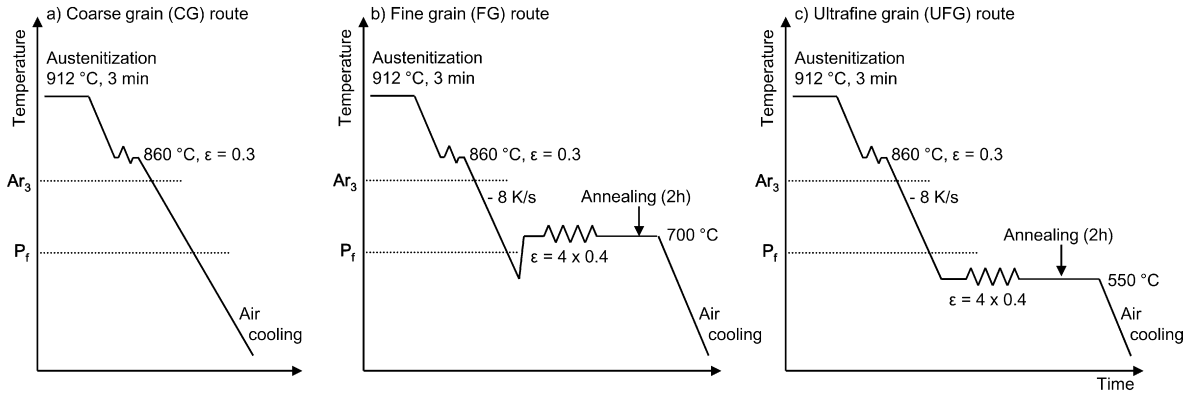

Fig. 1. Thermomechanical processing routes to produce different grain sizes in a hot deformation simulator. Ar_3: non-equilibrium transformation start temperature, P_f: pearlite transformation finish temperature, ε: logarithmic strain.

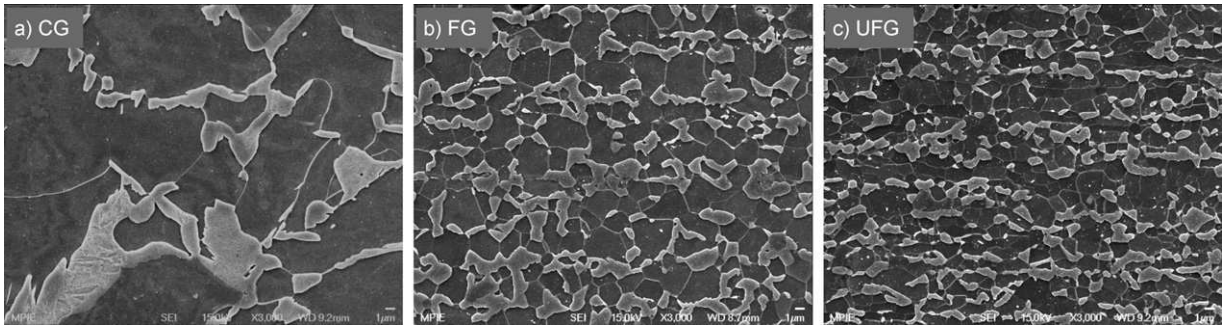

Fig. 2. Microstructures used to evaluate the effect of grain refinement on mechanical properties. The (a) coarse grained (CG), (b) fine grained (FG) and (c) ultrafine grained (UFG) material were produced by the processing routes illustrated in Fig. 1 plus intercritical annealing for 3 min at 730 °C in a salt bath, followed by water quenching. Rolling direction is horizontal, compression direction is vertical.

mainly isolated. Exemplary micrographs are shown in Fig. 2, the magnification being the same in all images.

As neither the chemical composition, nor the intercritical annealing temperature or holding time was changed, all three steels contain similar martensite fractions with presumably similar martensite carbon contents. Using a mass balance calculation, the martensite carbon content C_m can be estimated from the equation

$$C_m = \frac{C_c - C_f(1 - f_m)}{f_m} \quad (1)$$

where C_c is the carbon content of the composite, C_f is the carbon content of ferrite and f_m is the martensite volume fraction. The ferrite carbon content was estimated using Thermo-Calc [42]. It was assumed that upon water quenching, the ferrite keeps the carbon content which is present at the temperature where the austenite fraction is 30 vol.%. Thus, ferrite is supersaturated in carbon, the carbon content being 0.01 wt.%. Inserting this value in Eq. (1) yields a martensite carbon content of 0.54 wt.%.

Other authors conducting similar investigations [16,18] found that phase transformation kinetic is enhanced upon grain refinement. Hence, they report a higher martensite volume fraction in their UFG materials after the same intercritical annealing treatment. The reason why the martensite volume fraction is nearly the same for all grain sizes in the present case is probably the different processing route applied. Due to the pronounced recovery during large strain warm deformation [38], the stored energy in the initial microstructure might be lower than in the materials processed by ECAP [16] or cold swaging [18]. Hence, the driving force for phase transformation is not profoundly enhanced in the present case. This leads to the advantageous situation that in this study, the differences in the mechanical properties can be solely attributed to the different grain size and these effects are not overlaid by differences in martensite volume fraction. However, it will be shown in the following, that the martensite distribution and the crystallographic texture have a considerable influence on the mechanical behavior.

3.2. Tensile properties

Fig. 3 shows the engineering stress–strain curves of the coarse grained, the fine grained, and the ultrafine grained DP steels. For each material, the result of only one of the three tensile tests is shown, because the variations within each series are rather small. The steels show the typical behavior of as-quenched ferrite/martensite dual-phase steels: low elastic limit, absence of a distinct yield point, continuous yielding and high initial strain hardening rate. With decreasing grain size, the tensile strength is remarkably increased whereas uniform elongation and total elongation are only slightly affected.

Table 1
Microstructure parameters obtained from SEM micrographs and tensile data presented as average value of three tensile specimen for each group. MVF: martensite volume fraction, d_f: ferrite grain size, YS: 0.2% offset yield strength, UTS: ultimate tensile strength, UE: uniform elongation, TE: total elongation, RIA: reduction in area.

Steel	MVF (%)	d_f (μm)	YS (MPa)	UTS (MPa)	UE (%)	TE (%)	RIA (%)	Yield ratio	n (2%-UE)
CG	31.3	12.4	445	870	7.2	7.7	13.0	0.51	0.21
FG	30.1	2.4	483	964	7.4	8.9	18.7	0.50	0.18
UFG	29.8	1.2	525	1037	7.1	7.3	15.3	0.51	0.18

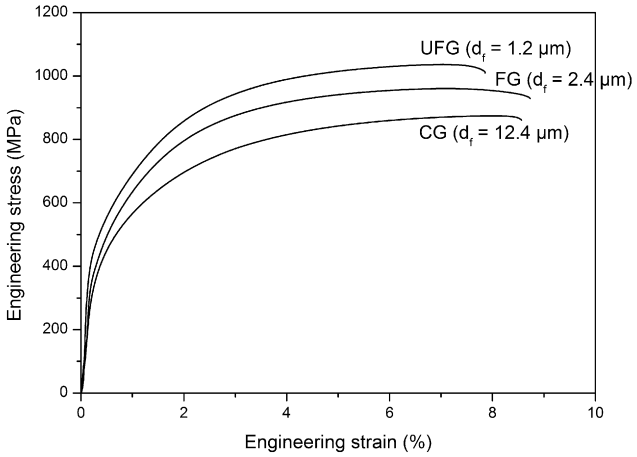

Fig. 3. Exemplary engineering stress–strain curves of the steels with coarse grained (CG), fine grained (FG) and ultrafine (UFG) ferrite matrix. Ferrite grain size (d_f) is given in brackets.

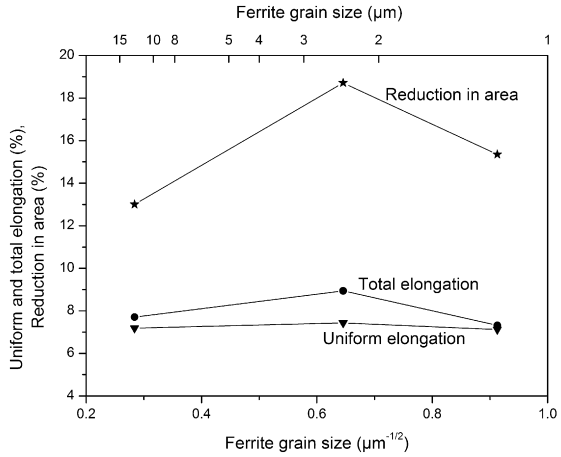

Fig. 5. Effect of grain refinement on ductility. The data points represent average values from three separate tensile tests for each steel.

Figs. 4–7 show average values for each steel obtained from three separate tensile tests which are listed in Table 1. The increase in yield strength (0.2% offset yield strength) and tensile strength (Fig. 4) follow a linear trend which was expected as the grain size and strength are related by a linear relationship given by the Hall–Petch equation ($\sigma_y = \sigma_0 + k_y d^{-1/2}$ where σ_y is the yield strength, d is the grain size, σ_0 is the friction stress required to move dislocations in a ferrite single crystal and k_y is the Hall–Petch slope quantifying the resistance against slip propagation across a grain boundary).

The grain size dependence (Hall–Petch coefficient) is 8.39 MPa/$d^{-1/2}$ (with d being the grain diameter in mm) for the tensile strength, and it is 4.0 MPa/$d^{-1/2}$ for the yield strength. These values are in the common range reported for dual-phase steels [43]. However, the Hall–Petch coefficient of the yield strength is lower than in ferrite/cementite steels that are refined to 1 μm and below [44]. This indicates that other phenomena like residual stresses and mobile dislocations, as described in the introduction, exert a strong influence on the yield strength of dual-phase steels. As yield and tensile strength are increased by about the same factor due to grain refinement, the yield ratio is nearly constant.

The effect of grain refinement on ductility is more complex than its effect on strength. The uniform elongation (Fig. 5) is nearly con-

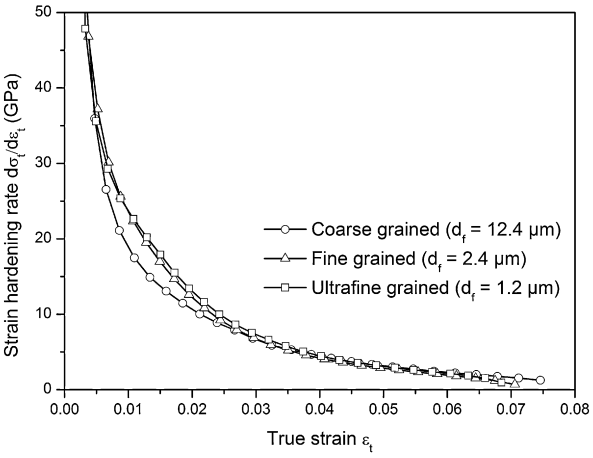

Fig. 6. Strain hardening rate as a function of true strain (average values from three tensile tests). Grain refinement increases the initial strain hardening rate. d_f: ferrite grain size.

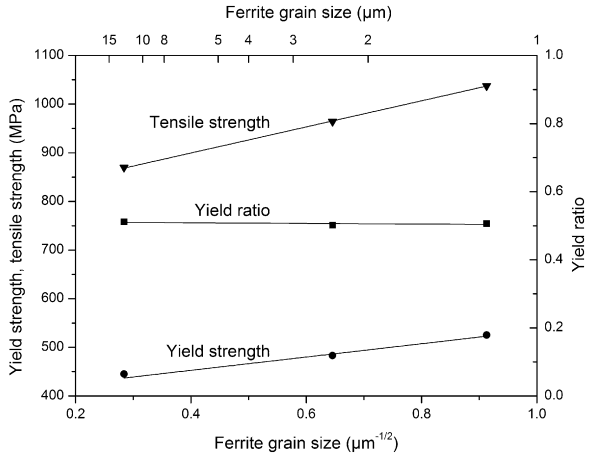

Fig. 4. Effect of grain refinement on yield strength (0.2% offset) and tensile strength. The data points represent average values from three separate tensile tests for each steel.

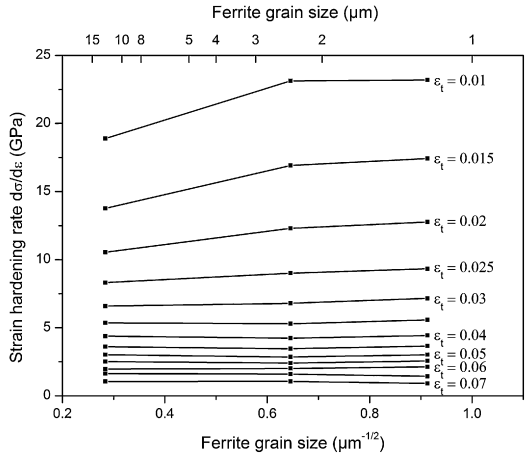

Fig. 7. Strain hardening rate at different true strain levels ε_t as a function of grain size, calculated as average values from three tensile test data.

stant around 7% for all steels. Both total elongation and reduction in area are highest in the FG steel. The UFG steel has a lower total elongation than the CG steel, but a higher reduction in area. However, the differences are rather small.

The analysis of the strain hardening rate (Fig. 6) reveals that the initial strain hardening rate is increased by grain refinement, but is nearly the same for the FG and the UFG steel. At higher strain levels, the two curves converge with the curve of the CG steel.

The effect of grain size on strain hardening behavior is more clearly revealed by plotting the average strain hardening rate of the three tensile specimens at different strain levels as a function of grain size, Fig. 7. It is obvious from this figure that grain refinement promotes initial strain hardening rate. At higher strains, the effect of grain refinement continuously decreases. At a true strain of around 0.07, the strain hardening rate of the ultrafine grained steel is slightly smaller than in the other steels. The n-value, calculated at strain levels between 2% and uniform elongation (Table 1), drops off slightly from 0.21 for the CG steel to 0.18 for the FG and UFG steel.

Fig. 8 shows the tensile specimens after failure. The post-uniform elongation increases with decreasing grain size which is clearly revealed by the more pronounced necking. The micrographs reveal the respective fracture modes of the steels. In case of the CG steel, it is mainly brittle, which is documented by well-defined facets and cleavage steps on these facets, Fig. 8a. Only some small areas consist of dimples. The latter are located in the martensitic area, whereas the ferrite exhibits cleavage planes. The dominant fracture mode of the FG steel is ductile, although smaller parts of the specimen have undergone brittle fracture, Fig. 8b. The UFG steel shows dimples throughout the specimens, Fig. 8c. This suggests a failure process of void nucleation and growth and hence, entirely ductile fracture. Some dimples are formed around inclusions which are probably manganese sulphides.

To find out the preferred void nucleation sites, surfaces perpendicular to the fracture surface were also analyzed. In the CG steel, the main fracture mechanism is martensite cracking. The cracks form mostly in the banded areas perpendicular to the applied tensile strain, Fig. 9a. The main part of the cracks stop at the ferrite/martensite interface, but some travel through a minor fraction of the adjacent ferrite grain. Martensite fracture was observed at strains as low as 3.4% plastic strain. Void nucleation and growth along ferrite/martensite interfaces occurs to a lesser extent within the areas of isolated martensite islands. In the FG and UFG steels, the voids form primarily at ferrite/martensite interfaces and are distributed more homogeneously, Fig. 9b. Martensite cracking takes place less frequently in martensite islands which exceed the average martensite island size and occurs only after necking has started.

3.3. Toughness

The Charpy impact curves for the CG, FG and UFG steel are depicted in Fig. 10a. In Table 2, both the raw data obtained from the subsize specimen (index "s") and the recalculated values for full size specimen (index 'C') are listed.

Both the upper shelf energy (USE) and the lower shelf energy (LSE) are enhanced continuously with ferrite grain refinement. The ductile-to-brittle transition temperature (DBTT), defined as the temperature at half USE, decreases from 127 °C for the CG steel to 100 °C for the FG steel and 94 °C for the UFG steel. This method of determining the transition temperature has the shortcoming that the microstructure is not taken into account. Therefore, the temperature at which the fracture mode is 50% brittle and 50% ductile (fracture appearance transition temperature, 50%-FATT), was determined additionally. While the 50%-FATT of the CG steel (132 °C) is similar to the value determined by the half USE (124 °C), it is 24 °C lower in case of the FG steel and 33 °C lower in the case of the UFG steel, Fig. 10b. This means that the FG steel and (more strongly) the UFG steel are able to deform plastically and therefore, to absorb more energy, at relatively low impact temperatures. This is reflected by the gradual decrease of the absorbed energy at low temperatures for the FG and UFG steel, Fig. 10a. In contrast, the curve of the CG steels exhibits a sharp drop in the absorbed energy between the USE and LSE.

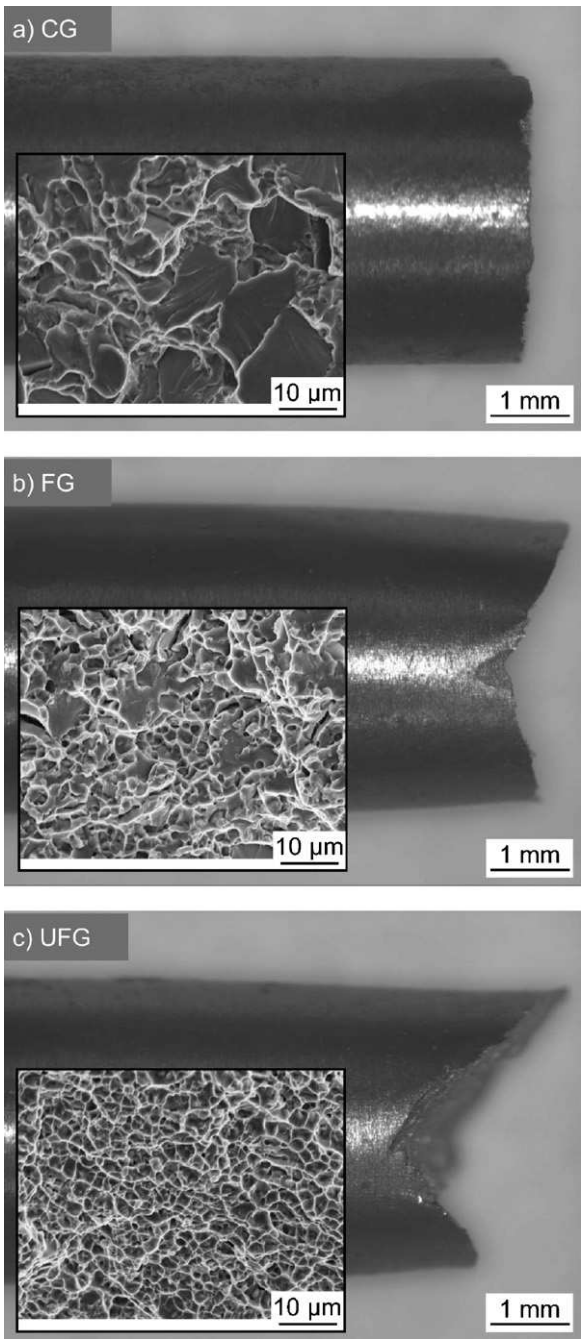

Fig. 8. Tensile specimen after failure showing the increase in post-uniform elongation with decreasing grain size and the promotion of ductile fracture mechanism.

Experimental evidence for the ability of the FG and UFG steel to deform plastically even close to the LSE is found by observing the fractured surfaces broken at room temperature, Fig. 11. While the CG steel fractures in a dominantly brittle manner, the UFG steel fails by void nucleation and growth. The main part of the FG steel shows ductile fracture as well, but some brittle fracture marks occur.

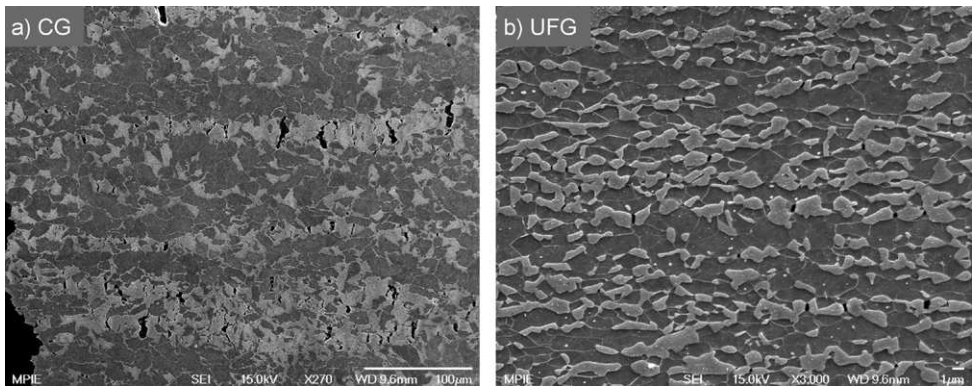

Fig. 9. Observation of the planes perpendicular to the fractured tensile specimen surfaces reveals (a) martensite cracking as the main fracture mechanism in the CG specimen and (b) void nucleation and growth in the UFG specimen. Note the different magnification of the images. The tensile direction is horizontal.

Both the FG and the UFG steel show some secondary fracture along the rolling direction (arrows in Fig. 11). This splitting phenomenon, sometimes referred to as delamination, is commonly observed in hot-rolled high strength steels and was found to exert a considerable effect on the energy absorption and on the DBTT [45].

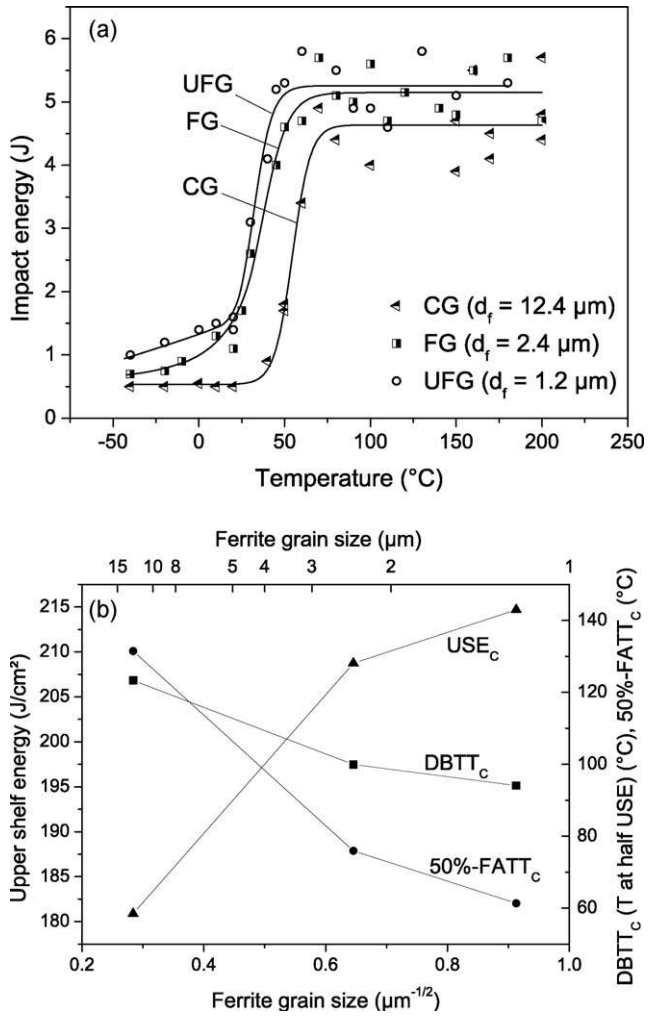

Fig. 10. Energy absorption curves obtained from subsize Charpy V-notch impact tests (a) and the impact data obtained by recalculating the values to full size specimen using the equations recommended by Kaspar and Faul [41] (b). USE: upper shelf energy, DBTT: ductile-to-brittle transition temperature, 50%-FATT: 50% ductile fracture appearance transition temperature, d_f: ferrite grain size.

It is seen that grain refinement enhances toughness in terms of both absorbed energy (USE and LSE) and transition temperature (T at half USE and 50%-FATT). The increase in toughness in the present case is due to the refinement of both ferrite and martensite, as the effective grain size in martensite (the coherent length of {0 0 1} plane in martensite packet) is also reduced [46]. In fact, it was calculated from EBSD scans that the average packet size (taking only HAGBs into account) is 0.9 µm in the CG steel and 0.5 µm in the UFG steel. A secondary reason for the deteriorated toughness of the CG steel is the partial banding of martensite, Fig. 9a. It was shown in previous studies that a fine distribution of martensite leads to improved impact properties when compared to fully banded microstructures [47].

4. Discussion

4.1. Strength and ductility

In general, the enhancement in strength due to grain refinement is accompanied by a deterioration of ductility. However, it was shown in previous studies [14–19] that this does not apply to DP steels. Instead, it was shown, that uniform and total elongation are only slightly affected by a decreasing ferrite grain size, as it is also observed in the present study. The grain size dependence of the mechanical properties is illustrated in Fig. 12. The data are in good agreement with the previous results. The differences in the Hall–Petch slopes result from the different processing routes and chemical compositions applied.

The increase in yield and tensile strength at roughly constant uniform and total elongation was explained with an increase in strain hardening rate with decreasing grain size [5,15,16,43]. A higher strain hardening rate delays the onset of necking and therefore, increases uniform elongation. Figs. 5–7 confirm these findings. Grain refinement increases strain hardening rate at low strains, at higher strains it levels off and equals the rate of the coarse grained reference material. This leads to a nearly unchanged uniform elongation with decreasing grain size. There are several explanations for this behavior. Firstly, the higher fraction of grain boundaries and heterophase interfaces increases the number of dislocation sources, giving rise to rapid increase in dislocation density and thus, strength [48]. Balliger and Gladman [5] further demonstrated that the strain hardening rate of DP steels is dependent on $(f/d)^{1/2}$ where f is the volume fraction of second phase and d is the mean second-phase diameter. Thus, at a constant martensite volume fraction, the strain hardening rate is increased with decreasing martensite island size. Son et al. [16] explain the increase in initial strain hardening rate due to grain refinement with the dislocation distribution in ferrite. In their coarse grained microstructure, the dislocation density

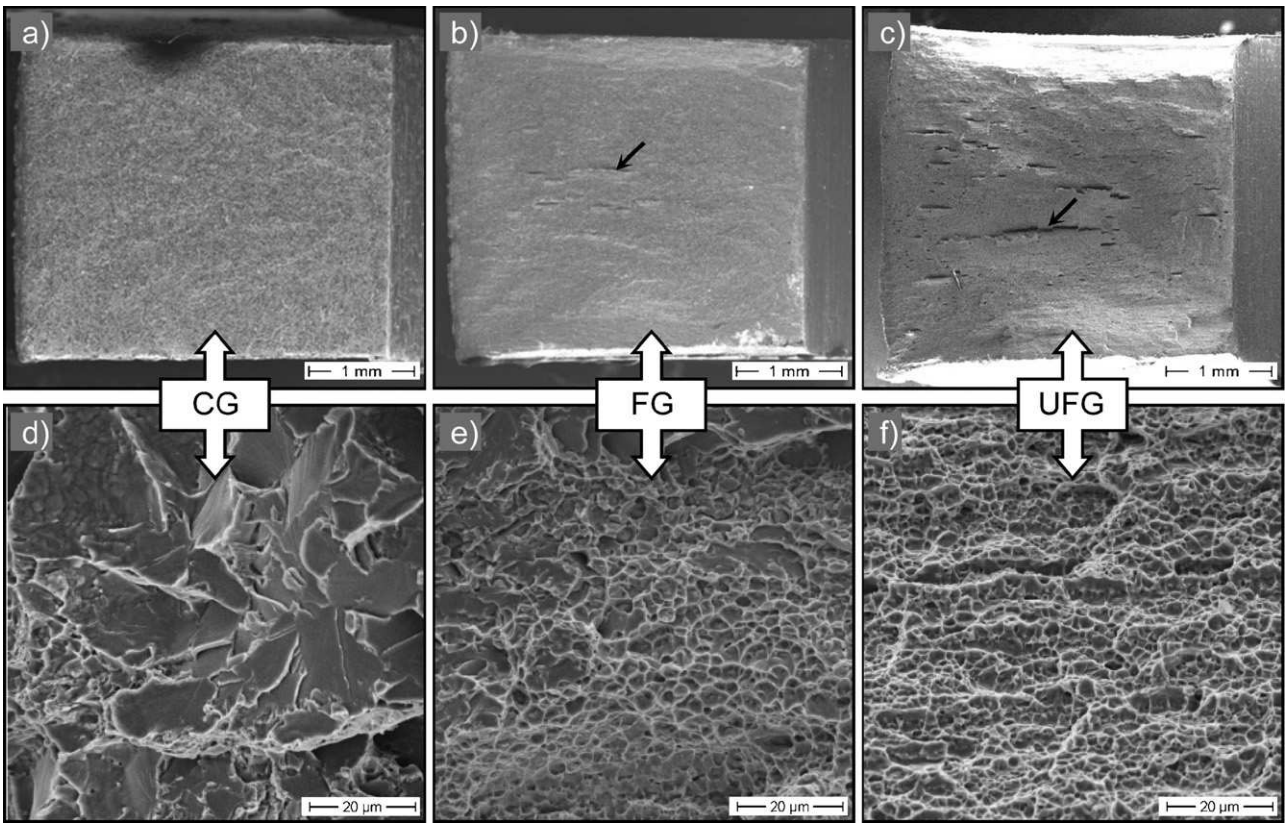

Fig. 11. Fracture surfaces of subsize Charpy impact specimen fractured at room temperature. Like in the tensile specimen, grain refinement promotes ductile failure. Some delamination occurs in the FG and the UFG specimen (arrows). Rolling direction is horizontal.

is very high close to the ferrite/martensite interface and low in the ferrite center, whereas in the ultrafine grained structure (~1 μm) it is high throughout the ferrite grains. Therefore, strain hardening by dislocation intersections is more rapid in the UFG microstructure. In fact, we observed [49] by using 3D-EBSD tomography, that ferrite grains smaller than 1 μm^3 can be entirely affected by the strain accommodation due to the martensitic phase transformation. In larger grains, the deformed zone does not extend to the ferrite grain interior. Therefore, we confirm the more homogeneous distribution of a high dislocation density described by Son et al. [16] for grains below 1 μm^3. Besides the stress increment due to rapid dislocation interaction as proposed by the authors, we assume that the plasticity of the ultrafine ferrite grains is restricted due to the high average dislocation density. Larger ferrite grains, which are always present in this type of microstructure, contain areas which are unaffected by the martensitic phase transformation. These grains will carry the main part of the strain during the initial stages of tensile straining, whereas the ultrafine ferrite grains will partly act as load carrying phase. Like the martensite phase, the ultrafine ferrite grains thus exert elastic back stresses due to the plastic incompatibility that contribute to the high initial strain hardening rate.

In view of low strain levels below 2%, it must be stated that the increase in yield strength due to ferrite grain refinement might affect the high initial strain hardening rate. Due to the absence of a distinct yield point, it is not possible to clearly distinguish between the effect of grain size on strain hardening rate and on yield strength. In this context, the investigation of the strain hardening rate after bake-hardening, i.e. after a heat treatment at 170 °C which leads to the reoccurrence of a yield point, would offer valuable information.

Another reason for the nearly constant uniform elongation with decreasing grain size might be the presence of small amounts (1–3 vol.%) of retained austenite in the UFG steel which is partly of isolated and partly of interlath type [35]. It was found from EBSD data that the amount of retained austenite is below 1% in the specimen area of uniform elongation and 0% in the necked area. That means, retained austenite transformed to martensite during tensile straining, supplying fresh dislocations to the microstructure which contribute to strain hardening and thus delay necking. This transformation induced plasticity (TRIP) effect is often considered to be negligible in DP steels because of the low volume fractions of retained austenite obtained, but was also shown to increase the uniform and total elongation due to an increase in strain hardening rate before the onset of necking [50–52]. In contrast to the UFG steel, the CG steel does not contain retained austenite. The stability of austenite is higher in the UFG steel due to (1) a size stabilization effect [4,53] and (2) a higher Mn content due to Mn enrichment during warm deformation [35]. Although the effect of retained austenite

Table 2
Charpy impact data obtained from the subsize specimen (index 's') and converted to values for full size Charpy V-notch (index 'C') specimen using the correlations given by Kaspar and Faul [41]. USE: upper shelf energy, DBTT: ductile-to-brittle transition temperature (temperature at 50% of USE), FATT: fracture appearance transition temperature.

Steel	USE_S (J)	USE_C (J/cm^2)	$DBTT_S$ (°C)	$DBTT_C$ (°C)	50%-$FATT_S$ (°C)	50%-$FATT_C$ (°C)
CG	4.6	181	53	123	60	131
FG	5.1	209	33	100	12.5	76
UFG	5.3	215	28	94	0	61

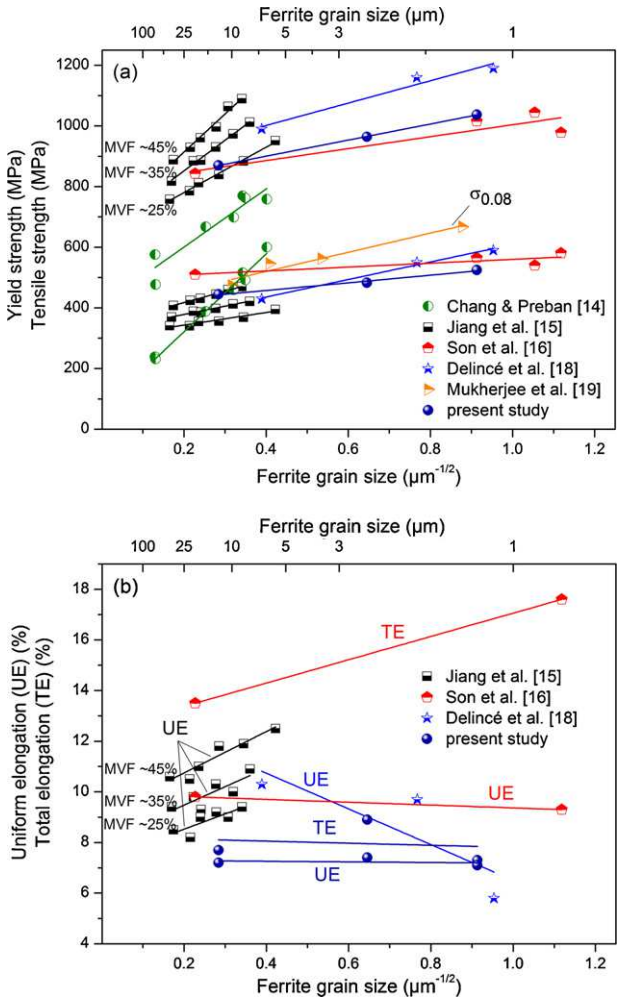

Fig. 12. Grain size dependence of (a) yield and tensile strength and (b) uniform and total elongation. MVF: martensite volume fraction, $\sigma_{0.08}$: flow stress at 8% strain, UE: uniform elongation, TE: total elongation.

transformation on the overall mechanical properties is presumably small, it should not be neglected.

4.2. Fracture mechanisms

The increased ductility due to grain refinement is reflected in the fracture mechanisms of the steels. At room temperature, the UFG steel shows ductile fracture mechanisms in response to both tensile and impact conditions, the CG steel shows mainly brittle behavior and the FG steel exhibits an intermediate fracture mechanism.

Brittle fracture behavior is favored due to martensite banding, large martensite island size and unfavorable distribution along ferrite grain boundaries in the CG steel. Voids and cracks are distributed mainly around martensite bands, Fig. 9a. Here, the local stress concentrations are highest as the stress relaxation by deformation of adjacent ferrite grains is restricted. As the plasticity of CG martensite is very low, premature martensite cracking or void nucleation at the interphase interface occurs. Martensite cracking is supported by the presence of former austenite–austenite grain boundaries which are known to be brittle due to their high susceptibility to segregations [54]. Moreover, it is possible that the banded martensite contains more carbon than the isolated martensite due to Mn segregation which acts as a sink for carbon. Therefore, it is likely that the banded martensite is less deformable and undergoes brittle fracture more easily. Davies [43] and Marder [55] found that martensite cracking is greatest when the carbon content is high and when the martensite is banded. As a consequence, premature martensite cracking controls both tensile strength and uniform elongation in the CG steel.

Kunio et al. [56] introduced the idea that connected martensite is the site of the incipient cracks which trigger cleavage in the ferrite. According to Uggowitzer and Stüwe [57], the fractured martensite acts as a sharp notch, leading to cleavage in ferrite. In the present case, martensite cracks are stopped by the ferrite in the CG steel but penetrate deeper into the ferrite grain with increasing strain. Close to the tensile strength, plastic constraints are too high to impede the crack penetration, and ferrite fails by cleavage. In the other steels, martensite cracking is less frequent and does not lead to ferrite cleavage fracture.

The fracture of martensite in the present study is at least in some parts of ductile nature, whereas the adjacent ferrite fails by cleavage. This fracture type was reported for DP steels previously [10,58,59]. As stress is transferred to martensite during tensile straining of DP steels, the fracture stress in martensite is reached much earlier than in ferrite. Therefore, ductile fracture of martensite is initiated. However, the initiated microcracks impose a high shear stress on the neighboring ferrite which increases with the martensite effective grain size. Hence, coarse martensite leads to cleavage fracture of ferrite, whereas the stresses produced by the fracture of fine or ultrafine martensite can be accommodated by plastic deformation of ferrite. Moreover, it is known that the plastic strain needed for the failure of a particle (or grain) increases with decreasing particle size. This behavior was repeatedly observed in DP steels [58,10] and is explained by the smaller number of dislocations piling-up at grain and phase boundaries which result in lower shear stresses. Kim and Thomas [60] found that coarse DP structures fracture predominantly by cleavage, while both fine fibrous and fine globular structures fracture in a ductile manner. They attribute this behavior to the constrained possibility of deformation localization in the fine structures which reduces the probability of cleavage crack nucleation in ferrite. The deformation mechanisms of ferrite and martensite are the subject of another paper recently submitted by our group.

The promotion of ductile fracture behavior is further revealed by the improved Charpy impact properties due to grain refinement, Fig. 10. Grain refinement increases the cleavage fracture stress by reducing the maximum size of a crack and thus, the stress at the crack tip. This leads to the decrease of the ductile-to-brittle transition temperature. Consequently, at low impact temperatures, the FG and the UFG material are capable of undergoing ductile fracture behavior more readily than the CG material, leading to a lower 50%-FATT temperature and an increase in the lower shelf energy (LSE). Additionally, texture effects might play an important role [25]. In the CG material, texture is nearly random, whereas the FG and UFG steels exhibit a strong bcc rolling texture due to large strain warm deformation. Furthermore, the ferrite grains are slightly elongated and inclusions are aligned with the rolling directions. These features promote the occurrence of delaminations within the rolling plane [26,61,62], as revealed in Fig. 11b and c. Delaminations were found to reduce the triaxial stress state at the head of a propagating crack and to blunt the crack tip when the crack and delaminations planes intersect [63]. Thus, more energy can be absorbed at lower temperatures.

At high impact test temperatures, it is obvious that the FG and UFG steel absorb more energy than the CG steel. The higher initial strain hardening rate of the FG and UFG steels might contribute to the higher upper shelf energy (USE). Yet, the scatter of the data is rather high. This may be caused by tempering effects. Therefore, a further interpretation of the grain size effect on the USE does not seem to be reasonable.

5. Conclusions

Three low carbon dual-phase steels with nearly constant martensite fraction around 30 vol.% martensite and different ferrite grain size (1.2, 2.4 and 12.4 μm) were produced by applying hot deformation and large strain warm deformation at different deformation temperatures, followed by intercritical annealing. Their mechanical properties were studied based on tensile and impact test data and microstructure observations. The main conclusions are:

- Grain refinement leads to an increase of both yield strength and tensile strength following a linear relationship of Hall–Petch type. Uniform elongation and total elongation are hardly affected. The initial strain hardening rate and the post-uniform elongation increase as the grain size decreases.
- The increase in the initial strain hardening rate due to grain refinement is attributed to early dislocation interactions, the high number of dislocation sources and the back stresses exerted by (1) martensite islands and (2) ultrafine ferrite grains below 1 μm^3. The presence of small amounts of retained austenite in the ultrafine grained steel might play a secondary role.
- Impact toughness is improved by grain refinement which is revealed by a lower ductile-to-brittle transition temperature and an increase in both upper and lower shelf energy.
- Grain refinement promotes ductile fracture mechanisms in response to both tensile and impact conditions. The formation of martensite cracks and cleavage fracture in ferrite is suppressed in the fine grained and the ultrafine grained steels due to the small size, the more homogeneous distribution and more spherical shape of martensite islands.

References

[1] H. Fischmeister, B. Karlsson, Z. Metallkd. 68 (1977) 311–327.
[2] R.G. Davies, Metall. Trans. A 10 (1979) 1549–1555.
[3] D.K. Matlock, G. Krauss, L.F. Ramos, G.S. Huppi, in: R.A. Kot, J.W. Morris (Eds.), Structure and Properties of Dual-phase Steels, The Metallurgical Society of AIME, New York, USA, 1979, pp. 62–90.
[4] J.M. Rigsbee, P.J. Vander Arend, in: A.D. Davenport (Ed.), Formable HSLA and Dual-phase Steels, The Metallurgical Society of AIME, New York, USA, 1979, pp. 58–86.
[5] N.K. Balliger, T. Gladman, Met. Sci. 15 (1981) 95–108.
[6] G.R. Speich, A.B. Miller, in: R.A. Kot, B.L. Bramfitt (Eds.), Fundamentals of Dual-phase Steels, The Metallurgical Society of AIME, New York, USA, 1981, pp. 279–304.
[7] D.L. Bourell, A. Rizk, Acta Metall. 31 (1983) 609–617.
[8] D.A. Korzekwa, D.K. Matlock, G. Krauss, Metall. Trans. A 15 (1984) 1221–1228.
[9] A.M. Sarosiek, W.S. Owen, Mater. Sci. Eng. 66 (1984) 13–34.
[10] Y.L. Su, J. Gurland, Mater. Sci. Eng. 95 (1987) 151–165.
[11] M. Sarwar, R. Priestner, J. Mater. Sci. 31 (1996) 2091–2095.
[12] O. Bouaziz, T. Iung, M. Kandel, C. Lecomte, J. Phys. IV 11 (2001) 223–231.
[13] F.M. Al-Abbasi, J.A. Nemes, Int. J. Mech. Sci. 45 (2003) 1449–1465.
[14] P.H. Chang, A.G. Preban, Acta Metall. 33 (1985) 897–903.
[15] Z.H. Jiang, Z.Z. Guan, J.S. Lian, Mater. Sci. Eng. A 190 (1995) 55–64.
[16] Y.I. Son, Y.K. Lee, K.T. Park, C.S. Lee, D.H. Shin, Acta Mater. 53 (2005) 3125–3134.
[17] P. Tsipouridis, E. Werner, C. Krempaszky, E. Tragl, Steel Res. Int. 77 (2006) 654–667.
[18] M. Delincé, Y. Brechet, J.D. Embury, M.G.D. Geers, P.J. Jacques, T. Pardoen, Acta Mater. 55 (2007) 2337–2350.
[19] K. Mukherjee, S.S. Hazra, M. Militzer, Metall. Mater. Trans. A 40A (2009) 2145–2159.
[20] R. Song, D. Ponge, D. Raabe, J.G. Speer, D.K. Matlock, Mater. Sci. Eng. A 441 (2006) 1–17.
[21] K. Mukherjee, S. Hazra, P. Petkov, M. Militzer, Mater. Manuf. Process. 22 (2007) 511–515.
[22] K.T. Park, Y.S. Kim, J.G. Lee, D.H. Shin, Mater. Sci. Eng. A 293 (2000) 165–172.
[23] N. Tsuji, N. Kamikawa, R. Ueji, N. Takata, H. Koyama, D. Terada, ISIJ Int. 48 (2008) 1114–1121.
[24] T. Hanamura, F. Yin, K. Nagai, ISIJ Int. 44 (2004) 610–617.
[25] R. Song, D. Ponge, D. Raabe, Acta Mater. 53 (2005) 4881–4892.
[26] Y. Kimura, T. Inoue, F. Yin, O. Sitdikov, K. Tsuzaki, Scripta Mater. 57 (2007) 465–468.
[27] S. Hayami, T. Furukawa, in: M. Korchynsky (Ed.), Microalloying 75 Proceedings of an International Symposium on High-Strength, Low-Alloy Steels, Union Carbide Corporation, New York, USA, 1977, pp. 311–320.
[28] G.R. Speich, R.L. Miller, in: R.A. Kot, J.W. Morris (Eds.), Structure and Properties of Dual-phase Steels, The Metallurgical Society of AIME, New York, USA, 1979, pp. 145–182.
[29] T. Sakaki, K. Sugimoto, T. Fukuzato, Acta Metall. 31 (1983) 1737–1746.
[30] Q.A. Chen, R. Kaspar, O. Pawelski, Z. Metallkd. 76 (1985) 348–352.
[31] J.M. Moyer, G.S. Ansell, Metall. Trans. A 6 (1975) 1785–1791.
[32] G. Tither, M. Lavite, JOM 27 (1975) 15–23.
[33] M. Grujicic, T. Erturk, W.S. Owen, Mater. Sci. Eng. 82 (1986) 151–159.
[34] R. Song, D. Ponge, D. Raabe, ISIJ Int. 45 (2005) 1721–1726.
[35] M. Calcagnotto, D. Ponge, D. Raabe, ISIJ Int. 48 (2008) 1096–1101.
[36] O. Pawelski, R. Kaspar, Materialprüfung 30 (1988) 357–360.
[37] R. Kaspar, O. Pawelski, Materialprüfung 31 (1989) 14–16.
[38] R. Song, D. Ponge, D. Raabe, R. Kaspar, Acta Mater. 53 (2005) 845–858.
[39] A. Belyakov, T. Sakai, H. Miura, R. Kaibyshev, K. Tsuzaki, Acta Mater. 50 (2002) 1547–1557.
[40] J.S. Distl, A. Streißelberger, R. Kaspar, U. Zeislmair, Materialprüfung 27 (1985) 131–135.
[41] R. Kaspar, H. Faul, Materialprüfung 43 (2001) 18–21.
[42] B. Jansson, M. Schalin, M. Selleby, B. Sundman, in: C.W. Bale, G.A. Irons (Eds.), Computer Software in Chemical and Extractive Metallurgy, The Metallurgical Society of CIM, Quebec, Canada, 1993, pp. 57–71.
[43] R.G. Davies, Metall. Trans. A 9 (1978) 671–679.
[44] K. Takeda, N. Nakada, T. Tsuchiyama, S. Takaki, ISIJ Int. 48 (2008) 1122–1125.
[45] M. Yang, Y.J. Chao, X. Li, D. Immel, J. Tan, Mater. Sci. Eng. A 497 (2008) 462–470.
[46] S. Morito, H. Saito, T. Ogawa, T. Furuhara, T. Maki, ISIJ Int. 45 (2005) 91–94.
[47] A. Bag, K.K. Ray, E.S. Dwarakadasa, Metall. Mater. Trans. A 30 (1999) 1193–1202.
[48] H. Mathy, J. Gouzou, T. Gréday, in: R.A. Kot, B.L. Bramfitt (Eds.), Fundamentals of Dual-phase Steels, The Metallurgical Society of AIME, New York, 1981, pp. 413–426.
[49] M. Calcagnotto, D. Ponge, E. Demir, D. Raabe, Mater. Sci. Eng. A 527 (2010) 2738–2746.
[50] A.K. Sachdev, Acta Metall. 31 (1983) 2037–2042.
[51] S. Sangal, N.C. Goel, K. Tangri, Metall. Trans. A 16 (1985) 2023–2029.
[52] M.H. Saleh, R. Priestner, J. Mater. Process. Technol. 113 (2001) 587–593.
[53] S. Takaki, K. Fukunaga, J. Syarif, T. Tsuchiyama, Mater. Trans. 45 (2004) 2245–2251.
[54] J. Becker, E. Hornbogen, P. Stratmann, Z. Metallkd. 71 (1980) 27–31.
[55] A.R. Marder, Metall. Trans. A 13 (1982) 85–92.
[56] T. Kunio, M. Shimizu, K. Yamada, H. Suzuki, Eng. Fract. Mech. 7 (1975) 411–417.
[57] P. Uggowitzer, H.P. Stüwe, Mater. Sci. Eng. 55 (1982) 181–189.
[58] X.J. He, N. Terao, A. Berghezan, Met. Sci. 18 (1984) 367–373.
[59] X.L. Cai, J. Feng, W.S. Owen, Metall. Trans. A 16 (1985) 1405–1415.
[60] N.J. Kim, G. Thomas, Metall. Trans. A 12 (1981) 483–489.
[61] C.M. Yen, C.A. Stickels, Metall. Trans. 1 (1970) 3037–3047.
[62] B.L. Bramfitt, A.R. Marder, Metall. Trans. A 8 (1977) 1263–1273.
[63] D.W. Kum, T. Oyama, J. Wadsworth, O.D. Sherby, J. Mech. Phys. Solids 31 (1983) 173–186.